



Get Clarity On Generics

Cost-Effective CT & MRI Contrast Agents



FRESENIUS
KABI

WATCH VIDEO

AJNR

The diagnosis of herniated intervertebral disks with MR imaging: a comparison of gradient-refocused-echo and spin-echo pulse sequences.

S Murayama, Y Numaguchi and A E Robinson

This information is current as of August 2, 2025.

AJNR Am J Neuroradiol 1990, 11 (1) 17-22
<http://www.ajnr.org/content/11/1/17>

The Diagnosis of Herniated Intervertebral Disks with MR Imaging: A Comparison of Gradient-Refocused-Echo and Spin-Echo Pulse Sequences

Sadayuki Murayama¹
Yuji Numaguchi^{1,2}
Arvin E. Robinson¹

Axial MR images of 65 lumbar disks with herniated nucleus pulposus imaged by gradient-refocused-echo (GRE) and spin-echo (SE) MR pulse sequences of high field strength were compared for diagnostic quality. The GRE pulse sequence of 200–400/15 (TR/TE) with a flip angle of 15–30° was selected as optimal because of its high signal-to-noise ratio and good contrast between CSF, nucleus pulposus, and bone. The GRE technique was confirmed to be more sensitive in detecting prolapsed disks than the SE technique, but was less sensitive in demonstrating extruded disks. The combination of axial GRE and SE resulted in high detectability of herniated nucleus pulposus on axial MR images.

Our results suggest that the GRE technique is an important adjunct to SE imaging in studying herniated nucleus pulposus.

AJNR 11:17–22, January/February 1990

MR imaging is established as a valuable diagnostic method for characterizing cervical and lumbar spine disorders [1]. In addition, a variety of new techniques, such as fast scan and multiangle slices, have been incorporated to provide better and more efficient diagnostic images [2–9]. The gradient-refocused-echo (GRE) technique of MR imaging is one such approach that has been applied to patients with cervical radiculopathy. Good results have been reported, citing the advantage that the thecal sac/disk interface is clearly visualized [2–5]. However, the efficacy of this technique for studying the lumbar spine has rarely been reported [7, 8].

In the present study, the GRE technique was used to evaluate prospectively axial images of the lumbar spine. Image quality of the herniated nucleus pulposus was compared with those of conventional spin-echo (SE) sequences. An experimental study designed to select an optimal GRE pulse sequence for the lumbar spine was performed by using theoretical calculations.

Materials and Methods

Experimental Study

Experimental investigation to determine the optimal pulse sequence of the GRE technique for the diagnosis of lumbar disk disorders was conducted prospectively. MR images were obtained on a GE Signa 1.5-T unit with a flat product surface coil (10 × 6 in.). The following parameters were held constant for all images: 256 × 128 matrix, 20-cm field of view, 5-mm slice thickness, and four excitations.

One normal volunteer was studied with a GRE technique that employed variable TRs, TEs, and flip angles. Initially, TE was held at 15, and TRs of 50, 100, 200, 300, and 400 and flip angles at 5, 10, 15, 30, 45, and 60° were used. Subsequently, TRs and flip angles were held at 200 and 30°, respectively, and TEs of 13, 14, 15, 16, 17, and 18 were used. In this MR unit, the minimal TE was 13. A section of L4–L5 disk was imaged with these variable parameters.

Signal intensities (SI) of the CSF, disk material (nucleus pulposus), and bone of the neural arch were measured by means of a region-of-interest function. Noise was calculated by using

Received December 16, 1988; revision requested February 21, 1989; revision received May 25, 1989; accepted June 1, 1989.

Presented at the annual meeting of the American Society of Neuroradiology, Chicago, May 1988.

This work was supported in part by a grant from General Electric Company.

¹ Department of Radiology, Tulane University Medical Center, 1430 Tulane Ave., New Orleans, LA 70112. Address reprint requests to S. Murayama.

² Present address: Department of Diagnostic Radiology, University of Maryland Medical System, Baltimore, MD 21201.

0195–6108/90/1101–017
© American Society of Neuroradiology

a formula previously reported [10]. Equal areas were used for SI calculation of the CSF and disk material, and for area-to-noise calculation. The signal-to-noise ratio was calculated for CSF and disk material by using a formula previously reported [10]. Contrast between CSF and disk material was calculated by using the formula:

$$(\text{SI CSF} - \text{SI disk material}) / \text{SI disk material}$$

Contrast between disk material and bone was calculated by using the formula:

$$(\text{SI disk material} - \text{SI bone}) / \text{SI bone}$$

Clinical Study

An optimal GRE pulse sequence was selected on the basis of the experimental study, and its clinical efficacy was evaluated. About 300 patients thought to have lumbar spine disorders were examined at 1.5 T. All patients were imaged in the sagittal and axial planes with a flat product surface coil (10 × 6 in.). Sagittal images were obtained with T1-weighted, 500/20, and multiple-echo techniques with a longer TR, 2000–2500/30, 70, SE technique with one or two excitations.

Relative proton-density-weighted SE images, 1400–2000/30, were used for axial planes with two excitations. T2-weighted SE images, 1400–2000/70–80, were also used for axial planes in half the cases. Axial planes were obtained by using a multiple-angle, multiplanar technique that provided an independent choice of obliquity and position for each slice.

A GRE technique was used for tilted axial planes of selected lumbar disks in question. GRE images were obtained by using the optimal technique in our experimental study, 200–400/15, a flip angle of 15–30°, and four excitations. A flip angle of 30° was used in most cases. The matrix was 256 × 128 with an 18- or 20-cm field of view for both SE and GRE techniques in the axial plane. The section thickness was 5 mm.

The diagnosis of herniated nucleus pulposus was made by using sagittal SE images. The diagnostic criteria were as follows: (1) definite focal extrusion of the disk material into the epidural space; (2) disruption of the outer anulus fibrosus and/or posterior longitudinal

ligament; and (3) increased SI of the displaced disk material. Definite bulging anulus fibrosus without herniated nucleus pulposus and extremely degenerated disks were excluded. Interpretation of the images was made in a blind fashion by three experienced neuroradiologists. Good correlation of MR images with surgical findings was obtained in 29 cases. Fifteen of 36 patients with nonoperated herniated nucleus pulposus had axial CT imaging. Good correlation of MR images with axial CT images in these cases was also obtained. Twenty-one cases of nonoperated herniated nucleus pulposus were evaluated solely on the basis of MR as described above.

Patients with herniated nucleus pulposus were classified into two groups, those with prolapsed disks and those with extruded disks (including sequestered disks) (Fig. 1), on the basis of the classification scheme described by Masaryk et al. [11]. A prolapsed disk was represented by slight protrusion of a nucleus pulposus of high intensity on T2-weighted images. This was posteriorly bounded by a hypointense outer anulus fibrosus and posterior longitudinal ligament (Fig. 1A). Another type of prolapsed disk demonstrated slight protrusion of the nucleus pulposus with minimal disruption of the outer anulus fibrosus. An extruded disk, on the other hand, was represented by a large anterior extradural defect caused by an obvious rupture of the outer anulus fibrosus and/or posterior longitudinal ligament (Fig. 1B).

Altogether, 65 cases of herniated nucleus pulposus, including 39 prolapsed and 26 extruded disks, were diagnosed. Axial images obtained with GRE and SE techniques were compared for their ability to provide clear demarcation of the posterior margin of a herniated nucleus pulposus. SI of herniated nucleus pulposus on GRE was also evaluated.

Results

Experimental Study

Signal-to-noise ratio was calculated by using variable TRs and flip angles at a TE of 15 (Fig. 2). The signal-to-noise ratio of disk material showed a peak at 15° or 30° in each TR sequence. Longer TRs (200–400) yielded higher signal/noise

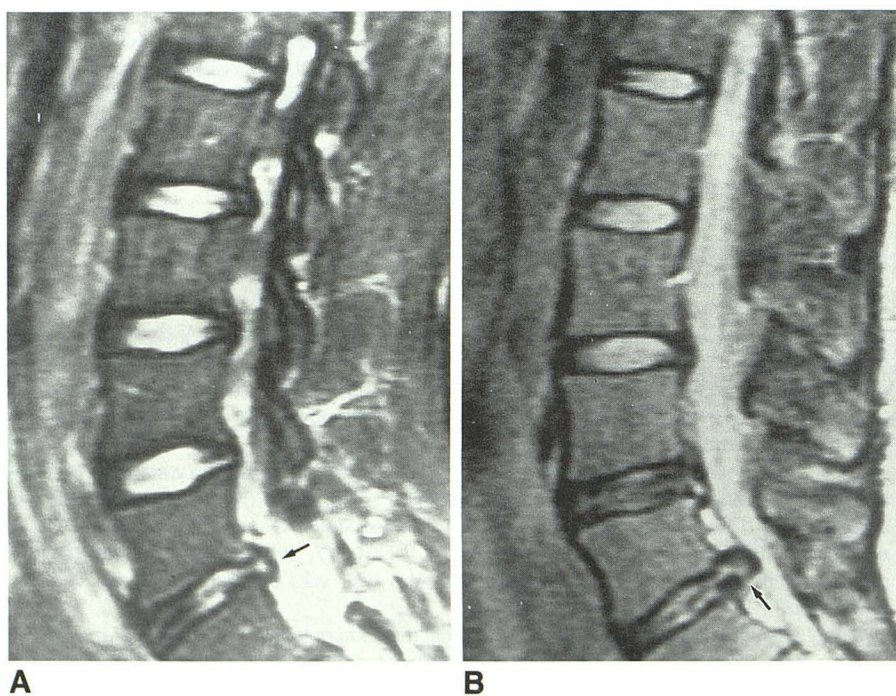


Fig. 1.—A, Prolapsed disk. T2-weighted sagittal image of lumbar spine shows small protrusion of disk material of high signal intensity at L5–S1 level (arrow). Protruded disk material is bounded by outer anulus fibrosus and posterior longitudinal ligament of low signal intensity posteriorly.

B, Extruded disk. T2-weighted sagittal image of lumbar spine shows large extradural mass contiguous with nucleus pulposus in disk. Inferior outer anulus fibrosus is disrupted (arrow).

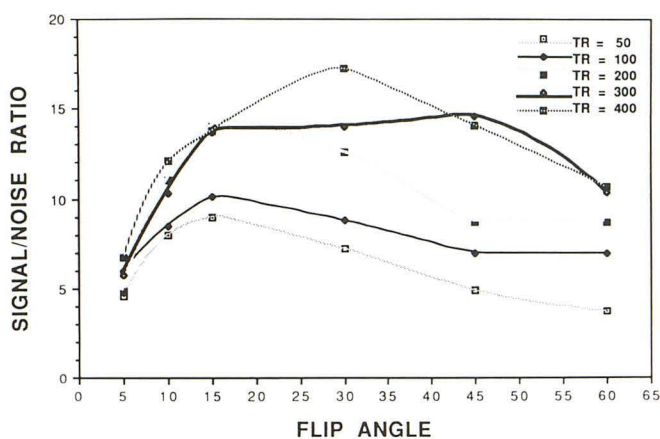
ratios of disk material. The signal-to-noise ratio of CSF, calculated by using long TRs (300–400), showed a peak at 45° or 60°. The signal/noise ratio of CSF at shorter TRs (50–200) showed a peak at 15° or 30°.

The contrast between CSF and disk material and between disk material and bone of the neural arch is shown in Fig. 3. The contrast between CSF and disk material showed a peak at 45° or 60° in each TR sequence. No significant increase or decrease of contrast was noted when the TR was increased. Contrast between disk material and bone showed a peak at 15° or 30° in each TR sequence. Longer TRs (200–400) yielded higher contrast than shorter TRs (50–100).

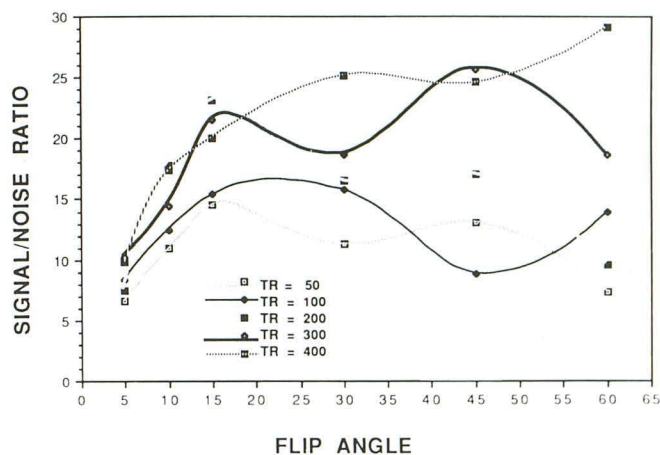
Images obtained at different TEs (13, 14, 15, 16, 17, and 18) with a TR of 200 and a flip angle of 30° are shown in Figure 4. No significant differences in contrast or signal/noise ratio were obtained. However, chemical shift cancellation artifacts were least prominent at a TE of 15.

Clinical Study

Table 1 compares the image quality of 65 axial GRE and SE studies. Herniated nucleus pulposus was detected in 54 disks (83%) by the GRE technique and in 52 disks (80%) by the SE technique. Fifty-nine herniated disks (91%) were detected on either axial GRE or SE images.

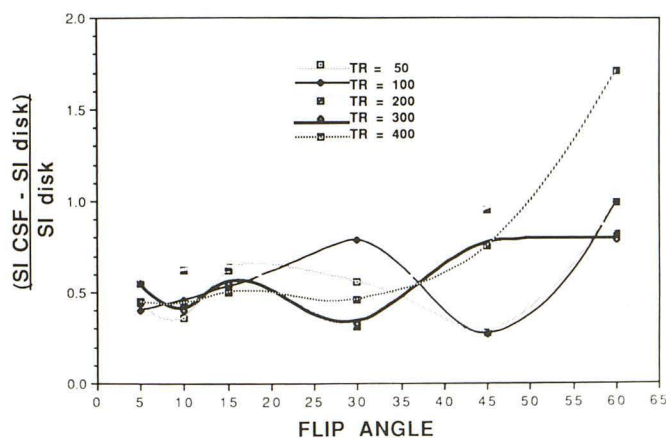


A

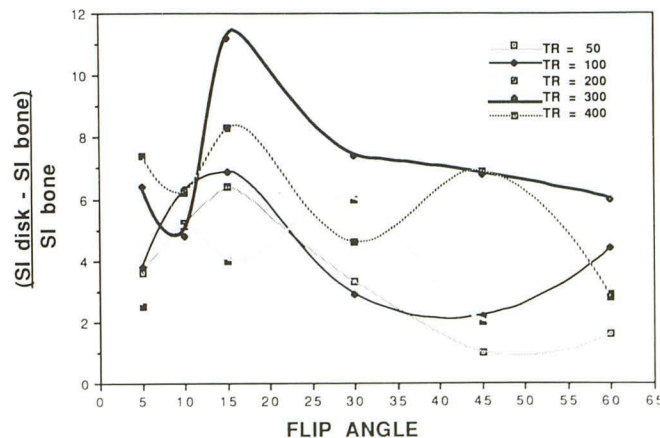


B

Fig. 2.—A, Signal/noise ratio of disk material as function of flip angle and TR. B, Signal/noise ratio of CSF as function of flip angle and TR.



A



B

Fig. 3.—A, Contrast between CSF and disk as function of flip angle and TR. B, Contrast between disk and bone as function of flip angle and TR.

Prolapsed disks were better shown in 20 (51%) of the 39 cases when using a GRE rather than an SE technique (Fig. 5). In five (13%) of the prolapsed disks, SE images were superior to those of GRE. On the other hand, extruded disks were better shown in 12 (46%) of the 26 cases when using an SE rather than a GRE technique (Fig. 6). In five extruded disks (19%), GRE images were superior to those of SE.

Herniated disk material in 14 (54%) of 26 extruded disks had SI that was higher than normal nucleus pulposus at the center of the disk and the same as CSF.

Discussion

Sagittal MR images are effective in showing herniated nucleus pulposus, but axial images are necessary for showing eccentricity and extent of narrowing of the spinal canal and neural foramen resulting from herniated nucleus pulposus. Although the quality of axial images has improved, conventional MR images are not considered comparable to that of high-resolution CT [8, 9, 12–14].

Our experimental study was designed to select an optimal pulse sequence with good signal-to-noise characteristics. Adequate contrast between CSF, disk material, and bone was also investigated, because diagnosis of lumbar herniated

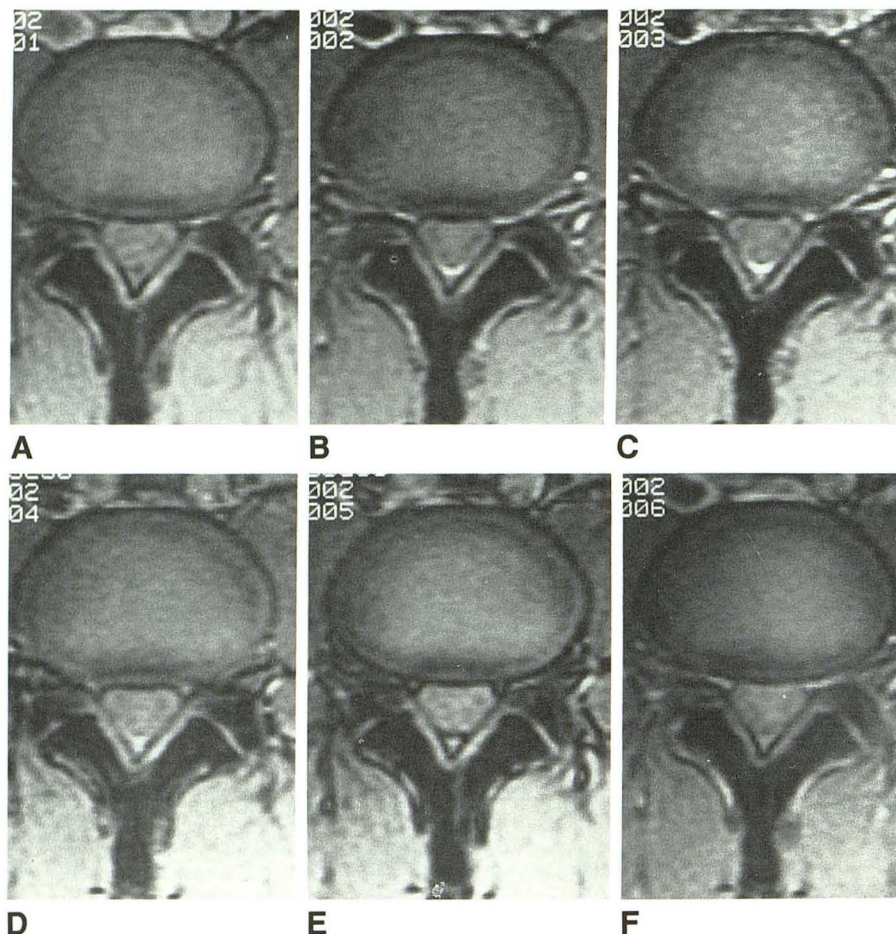


Fig. 4.—A–F, Series of axial images at TE = 13 (A), TE = 14 (B), TE = 15 (C), TE = 16 (D), TE = 17 (E), and TE = 18 (F). TR and flip angle were held constant at 200 and 30°, respectively.

nucleus pulposus requires clear identification of CSF, disk material, and bone. The SI of the GRE technique is determined by the TR, T1, T2*, and flip angle. The flip angle for optimal signal/noise is called the Ernst angle [2, 15, 16] (see the appendix). Our experimental study is equivalent to an investigation of Ernst angles for CSF and disk in each sequence. The signal/noise ratio of disk material in each TR sequence and of CSF in shorter TR sequences (50–200) showed a peak at 15° or 30°. This indicated that Ernst angles for these sequences were about 15° or 30°. Ernst angles of CSF at longer TR sequences (300–400) are considered to be about 45° or 60°. This result is consistent with the theory that the Ernst angle increases as TR increases.

Images of flip angles at 5° and 10° had more noise than did those at larger flip angles. Although images at flip angles of 5° and 10° are T2*-weighted, with CSF and disk material of high SI, the signal/noise ratio of CSF and disk material was considered inadequate.

For intermediate fast scans, a TR of 200–400 and flip angles of 15–30° result in mild to moderate T2* weighting, theoretically [15]. This imaging procedure showed good signal/noise for CSF and disk material. Good contrast between CSF, disk material, and bone was also obtained when using flip angles of 15° and 30° and a longer TR technique.

The images at longer flip angles (45° and 60°) had low noise. The good contrast we obtained between CSF and disk

TABLE 1: Detectability of Herniated Nucleus Pulposus by GRE and SE

Results of Diagnostic Sequence	Prolapsed Disk	Extruded Disk	Total
GRE alone, not seen on SE	6	1	7
GRE better than SE	14	4	18
GRE same as SE	10	7	17
SE better than GRE	2	10	12
SE alone, not seen on GRE	3	2	5
No herniated nucleus pulposus detected	4	2	6
Total	39	26	65

material is compatible with the results reported by Buxton et al. [16]. However, this sequence could not produce contrast between disk material and bone that was as good as that obtained with flip angles of 15° and 30°.

We did not study sequences with long TEs because longer TEs degraded image quality as a result of magnetic susceptibility effects [17]. Instead, we looked to significant differences between variably short TE parameters. A variable TE was supposed to yield in-phase and out-of-phase images by creating differences in the Larmor equation for fat and water. Out-of-phase images were expected to be better because

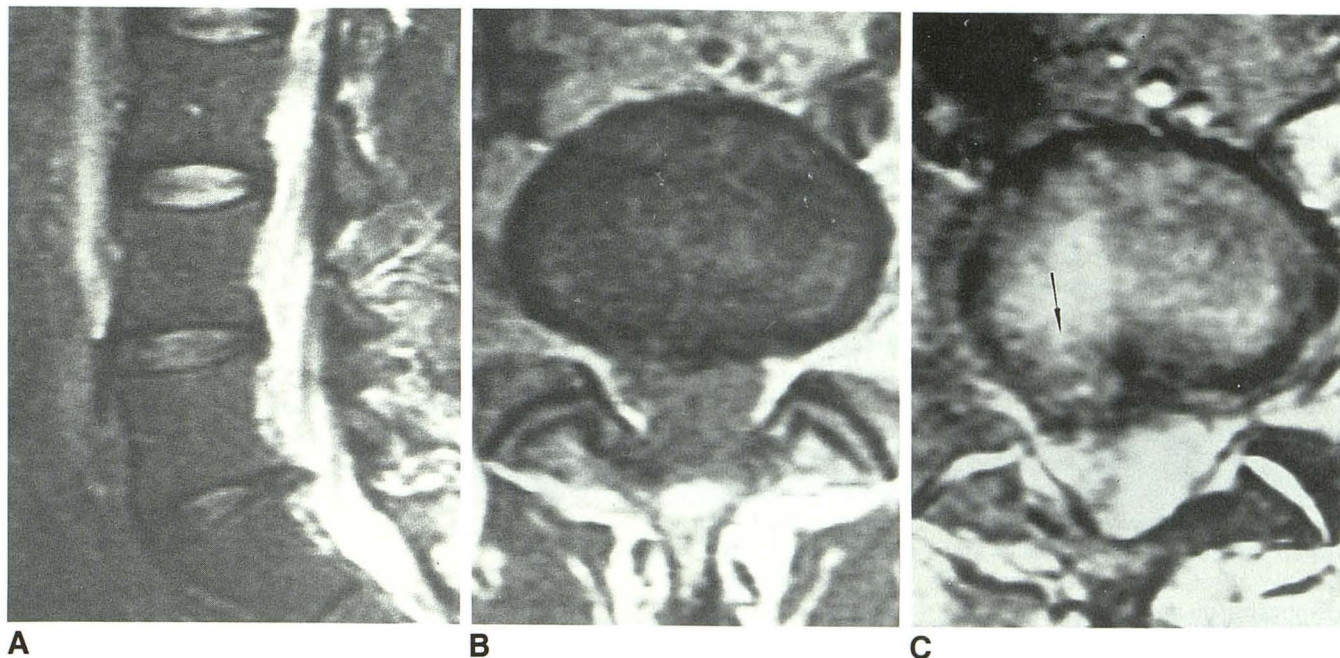


Fig. 5.—A, T2-weighted sagittal image (2000/70) of prolapsed disk in right lateral recess at L5–S1 level. B, On axial SE image (1400/30), focal protrusion into thecal sac was unclear. C, Diskographic effect. GRE image (400/15/30°) clearly demonstrates focal pathway (arrow) of herniated nucleus pulposus.

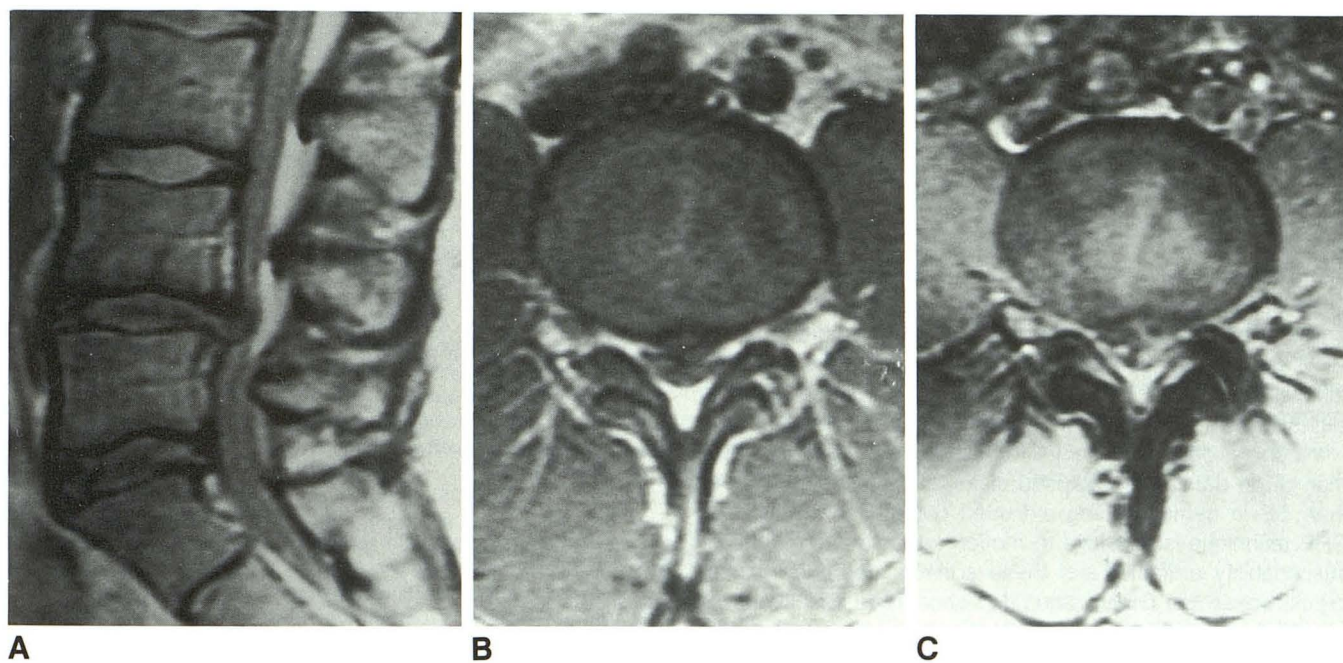


Fig. 6.—A, Proton-density-weighted sagittal image (2000/30) of extruded disk at L4–L5 level. B, Extruded disk obvious on a sagittal image is clearly visualized on axial SE image (1400/30). C, On axial GRE image (200/15/30°), the disk/thecal sac interface is less clear than on SE image.

they can highlight the signal of water in the herniated nucleus pulposus on a black background of bone marrow [18]. However, bone marrow signal from any TE sequence was markedly decreased. Bone marrow consists of trabecula interspersed with bone, and red and yellow marrow. This honey-comblike structure causes local field inhomogeneity, leading to rapid T2* dephasing. The T2* value of the vertebral body is approximately 10; therefore, the bone marrow appears

black when using a TE longer than 10 [19]. Because of this effect, contrast and signal/noise ratio were not significantly altered by any TE setting in this study. However, images at a TE of 15 showed the least chemical shift cancellation artifacts and were selected as optimal.

In accordance with these experimental results, we selected a TR of 200–400, a TE of 15, and a flip angle of 15–30° as the optimal imaging sequence for the lumbar spine.

In the clinical study, we classified herniated nucleus pulposus as prolapsed or extruded disks. Prolapsed disks were occasionally difficult to distinguish from bulging disks. Therefore, we used two diagnostic criteria for prolapsed disks: (1) a hyperintense prolapsed nucleus pulposus on T2-weighted images, and (2) a disrupted anulus fibrosus [11].

Axial GRE was more sensitive in detecting prolapsed disks than was axial SE. A prolapsed disk usually appears as a small focal extrusion of the disk plane in conventional SE images and is expected to be of high intensity on T2-weighted images. However, T2-weighted SE images were less effective than expected. The high signal/noise ratio of our GRE technique assisted in demonstrating prolapsed disks that were only small protrusions on axial images. In addition, the GRE technique occasionally demonstrated the pathway of the herniated nucleus as high-intensity areas (Fig. 5). This diskographic effect by the GRE technique also was helpful in demonstrating prolapsed disks.

On the other hand, extruded disks were more easily demonstrated on axial SE images. Typical focal extrusion of the disk material was clearly visualized. However, on axial GRE images, focal extrusions of five cases were difficult to demonstrate because the disk/thecal sac interface was unclear. Extruded disks show disruption of the anulus fibrosus and/or posterior ligament, and the actual disk/thecal sac interface becomes a thin structure. Thus, if there is not adequate contrast between extruded nucleus pulposus and CSF, the disk/thecal sac interface becomes unclear. On GRE images, the extruded nucleus pulposus had a tendency to have a higher intensity than the normal nucleus pulposus and was of low contrast compared with CSF. The disk/thecal sac interface becomes unclear because of the same phenomenon. Flip angles of 45° and 60°, which were confirmed to yield more contrast between CSF and disk material by the experimental study, may provide better images of extruded disks.

In four cases, sequestered disks were overlooked on axial GRE images because the GRE technique was applied only for disk planes. This disadvantage can be avoided if slices slightly above and below the disk planes are obtained.

In conclusion, our present GRE technique is more sensitive than SE in detecting prolapsed disks, but it is less sensitive than SE in demonstrating extruded disks. Reportedly, the GRE technique is sensitive to motion artifacts and magnetic susceptibility artifacts, and these artifacts degrade images [3]. However, our GRE images do not seem to be influenced critically by those artifacts, and anatomic details were readily identified because of a high signal/noise ratio. Our results show that the combination of axial GRE and SE provided 90% sensitivity in demonstrating herniated nucleus pulposus. An improved GRE technique will be an even more important adjunct to SE images in future studies of this disorder.

Appendix

The image intensity S in GRE image is calculated by

$$S = \frac{SO \sin(\theta)[1 - \exp(-TR/T1)]\exp(-TE/T2^*)}{1 - \exp(-TR/T1)\cos(\theta)}$$

where SO is proton density and θ is a flip angle.

Ernst angle, the flip angle that optimizes signal/noise ratio, can be given by

$$\cos(\alpha) = \exp(-TR/T1)$$

where α is the Ernst angle.

ACKNOWLEDGMENTS

We thank Terry McGuckin and Geraldine Brooks for secretarial assistance, and Richard Hutton and John Geshner for technical assistance.

REFERENCES

1. Norman D. The spine. In: Brant-Zawadzki M, Norman D, eds. *Magnetic resonance imaging of the central nervous system*. New York: Raven Press, 1987:289-328
2. Winkler ML, Ortendahl DA, Mills TC, et al. Characteristics of partial flip angle and gradient reversal MR imaging. *Radiology* 1988;166:17-26
3. Enzmann DR, Rubin JB. Cervical spine: MR imaging with a partial flip angle, gradient-refocused pulse sequence. Part I. General considerations and disk disease. *Radiology* 1988;166:467-472
4. Wehrli FW, Shimakawa A, Gullberg GT, Macfall JR. Time-of-flight MR flow imaging: selective saturation recovery with gradient refocusing. *Radiology* 1986;160:781-785
5. Hedberg MC, Drayer BP, Flom RA, Hodak JA, Bird CR. Gradient echo (GRASS) MR imaging in cervical radiculopathy. *AJNR* 1988;9:145-151
6. Wantanabe AT, Teitelbaum GP, Bradley WG, Whittmore AR. Comparison of gradient-echo and spin-echo transaxial imaging of the lumbar spine. Presented at the twenty-sixth annual meeting of the American Society of Neuroradiology, Chicago, May 1988
7. Mark AS, Atlas SW, Fram EK. Fast scanning of lumbar spine disease: comparison with spin echo MR imaging and clinical applications. Presented at the twenty-sixth annual meeting of the American Society of Neuroradiology, Chicago, May 1988
8. Reicher MA, Lufkin RB, Smith S, et al. Multiple-angle, variable-interval, nonorthogonal MRI. *AJR* 1986;147:363-366
9. Reicher MA, Gold RH, Halbach VV, Rauschnig WR, Wilson GH, Lufkin RB. MR imaging of the lumbar spine: anatomical correlations and the effects of technical variations. *AJR* 1986;147:891-898
10. Enzmann DR, O'Donohue J. Optimizing MR imaging for detection of small tumors in the cerebellopontine angle and internal auditory canal. *AJNR* 1987;8:99-106
11. Masaryk TJ, Ross JS, Modic MT, Boumprey F, Bohlman H, Wilber G. High-resolution MR imaging of sequestered lumbar intervertebral disks. *AJNR* 1988;9:351-358, *AJR* 1988;150:1155-1162
12. Edelman RR, Shoukimas GM, Stark DD, et al. High-resolution surface-coil imaging of lumbar disk disease. *AJNR* 1985;6:479-485
13. Modic MT, Masaryk T, Boumprey F, Goormastic M, Bell G. Lumbar herniated disk disease and canal stenosis: prospective evaluation by surface coil MR, CT, and myelography. *AJNR* 1986;7:709-717, *AJR* 1986;147:757-765
14. Berger PE, Akinson D, Wilson WJ, Wiltse L. High resolution surface coil magnetic resonance imaging of the spine: normal and pathologic anatomy. *RadioGraphics* 1986;6:573-602
15. Wehrli FW. Principles of magnetic resonance. In: Stark DD, Bradley WG, eds. *Magnetic resonance imaging*. St. Louis: Mosby, 1988:3-23
16. Buxton R, Edelman RR, Rosen BR, Wismer GL, Brady TJ. Contrast in rapid MR imaging: T1- and T2-weighted imaging. *J. Comput Assist Tomogr* 1987;11:7-16
17. Edelman RR, Johnson K, Buxton R, et al. MR of hemorrhage: a new approach. *AJNR* 1986;7:751-756
18. Axel L. Chemical shift imaging. In: Stark DD, Bradley WG, eds. *Magnetic resonance imaging*. St. Louis: Mosby, 1988:229-243
19. Haacke EM, Tkach JA, Parrish TB. Reduction of T2* dephasing in gradient field-echo imaging. *Radiology* 1989;170:457-462